This paper appears in *Remote Sensing of Environment*, 2015, DOI: http://dx.doi.org/10.1016/j.rse.2014.09.034. The document below represents the final revision (preprint) submitted to the journal prior to publication.

SAR and optical remote sensing: assessment of complementarity and interoperability in the context of a large-scale operational forest monitoring system

Eric A. Lehmann[1,*], Peter Caccetta[1], Kim Lowell[2], Anthea Mitchell[3], Zheng-Shu Zhou[1], Alex Held[4], Tony Milne[3] and Ian Tapley[5]

[1] Commonwealth Scientific and Industrial Research Organisation (CSIRO), Digital Productivity Flagship, Private Bag 5, Wembley WA 6913, Australia (Eric.Lehmann@csiro.au, Peter.Caccetta@csiro.au, Zheng-Shu.Zhou@csiro.au)
*Corresponding author: Tel. +61 (0)8 9333 6123, Fax. +61 (0)8 9333 6121
[2] Cooperative Research Centre for Spatial Information (CRC-SI), University of Melbourne, Carlton, VIC, Australia (klowell@unimelb.edu.au)
[3] CRC-SI, The University of New South Wales, Sydney, NSW, Australia (a.mitchell@unsw.edu.au, t.milne@unsw.edu.au)
[4] CSIRO Land and Water, Canberra, ACT, Australia (Alex.Held@csiro.au)
[5] CRC-SI, Perth, Australia (hgciant@bigbond.net.au)

Abstract

In light of the growing volumes of remote sensing data generated by multiple space-borne platforms, integrated multi-sensor frameworks will continue to generate significant interest in the frame of international forest monitoring initiatives. This work investigates the interoperability of synthetic aperture radar (SAR) and optical datasets for the purpose of large-scale and operational forest monitoring. Using a discriminant technique known as canonical variate analysis, we investigate the level of discrimination (between forest and non-forest training sites) achieved by different datasets, thereby providing an assessment of complementarity between Landsat data and SAR data acquired at C-band (RADARSAT-2) and L-band (ALOS PALSAR), as well as related texture measures. Spatio-temporal methods developed as part of Australia's Land Cover Change Program (an established forest mapping and carbon accounting scheme operating at continental scale) are subsequently used for the integration of Landsat and (segmented) PALSAR data. To highlight specific operational aspects of the multi-sensor framework, this approach is demonstrated over the Australian state of Tasmania (approximately 6.8 million hectares), one of several national demonstrator sites defined by the Forest Carbon Tracking task of the Group on Earth Observations (GEO-FCT). In terms of complementarity, the combination of Landsat and L-band SAR data is found to provide most of the forest discrimination, while texture information and single-date C-band SAR data are found to provide only limited additional discrimination improvement in the frame of the considered monitoring system. The interoperability of optical and SAR data is assessed by comparison of forest maps resulting from the spatio-temporal processing under different scenarios, including: *i)* Landsat-only time series, *ii)* PALSAR-only time series, and *iii)* mixed Landsat – PALSAR time series. A comparison of the single-date optical and SAR-based forest classifications indicates a good agreement over Tasmania, with some bias towards forest in the PALSAR classifications. Significant differences are evident when considering the case of forest conversion (deforestation and afforestation) over large areas, thereby compromising the full interoperability of SAR and optical data within the framework of Australia's carbon accounting system.

Keywords: Landsat, ALOS PALSAR, RADARSAT-2, linear discriminant analysis, canonical variate analysis, conditional probability network, forest carbon tracking.

1. Introduction

1.1. Background

Remote sensing data acquired by space-borne platforms are of paramount importance for systems aiming to provide large-scale mapping and monitoring of forest extents (DeFries et al., 2007). Together with historical time series of (mostly optical) data extending back to the 1970s, sensors based on technologies such as synthetic aperture radar (SAR) provide opportunities for enhanced monitoring of the changing extents of the world's forest resources. Initiatives such as the Forest Carbon Tracking task of the Group on Earth Observations (GEO-FCT), currently known as the Global Forest Observations Initiative (GFOI), aim to demonstrate that coordinated multi-sensor Earth observations can provide the basis for reliable

and consistent forest information services to support global forest carbon estimation and reporting systems, as part of the United Nations' Framework Convention on Climate Change (UNFCCC) and Reducing Emissions from Deforestation and Forest Degradation (REDD) agreements (Herold and Johns, 2007). Key aspects of data interoperability (obtaining the same thematic results with different sensors) and complementarity (adding thematic value by using two or more sensors) are therefore of specific interest in the development of such multi-sensor forest monitoring systems.

Taking advantage of the synergies between SAR and optical data has been the focus of many scientific studies in recent times (e.g., de Oliveira Pereira et al., 2013; Dong et al., 2013; Lisini et al., 2011; Morel et al., 2012; Wolter and Townsend, 2011). Such investigations draw on the complementary nature of SAR and optical data to extract enhanced information on a variety of environmental variables such as landcover, above-ground biomass, road networks, and crop types. Most of these works represent case studies where the proposed methods are applied to datasets that are relatively limited geographically, temporally, or both. While highly relevant locally, their applicability to broader geographical and temporal scales in operational settings thus remains generally untested.

Operational and large-scale monitoring of landcover already occurs in several parts of the world. Examples include the pan-European CORINE land database supplied by the European Environmental Agency (EEA, 2007), the National Land Cover Database in the USA (Homer et al., 2004), as well as the Land Cover Change Program as part of Australia's National Inventory (NI-LCCP; ADE, 2014). Due to the prevalence of optical sensors in earlier Earth observation datasets, most of these operational frameworks have been developed on the basis of optical data. There exist currently no continuous and operational SAR-based forest monitoring systems, although one notable endeavour is the recent publication of multi-annual (2007 to 2010) time series of global ALOS PALSAR mosaics (Shimada et al., 2011; Shimada and Ohtaki, 2010) by Japan's Aerospace Exploration Agency (JAXA). Shimada et al. (2014) demonstrate how a worldwide forest/non-forest (F/NF) map can be achieved on the basis of these mosaics through simple regional thresholding of the cross-polarised PALSAR data; as per the authors' comments, this information product will admittedly require further improvements, for instance, to account for each country's specific definition of forest (JAXA, 2014). More generally, approaches to multi-temporal data fusion of SAR and optical time series for the detection of forest change also remain limited at present time (Lu et al., 2014).

SAR – optical sensor interoperability thus remains an active research topic, and the present work is concerned with the integration of SAR and optical data time series in the operational context of a large-scale forest monitoring system. The approach used here relies on the processing methodologies developed within Australia's Land Cover Change Program (Caccetta et al., 2010, 2007; Furby, 2002). Using Landsat imagery, this framework offers the capacity for fine-scale mapping and monitoring of the extent and change in perennial vegetation at continental scale (approximately 769 million hectares), allowing for an effective estimation of the greenhouse gas emissions from land use and land use changes (Brack et al., 2006). It is updated on an annual basis and currently uses over 8,500 Landsat scenes re-sampled at a spatial resolution of 25 m for twenty-two epochs since 1972. Originally implemented over Australia, these methods are now also being rolled out in Indonesia as part of the Land Cover Change Analysis program, the remote sensing monitoring component of Indonesia's National Carbon Accounting System (LAPAN, 2014; Roswintiarti et al., 2013). Further NI-LCCP investigations under governmental schemes such as the International Forest Carbon Initiative (IFCI, administered by the Australian government in response to GEO-FCT) involve taking advantage of new technologies in the area of space-borne SAR sensors, in particular as a key alternative for Earth observations in tropical areas where cloud cover is prevalent (e.g. Indonesia). This operational system therefore represents an ideal candidate framework to assess the integration of SAR and optical data for large-scale forest monitoring.

The processing methods used within NI-LCCP allow for the integration of data from different sensors. For instance, Furby and Wu (2009) investigate the issues involved with the use of SPOT 4 and Landsat 7 data as part of the (at the time) existing Landsat 5 time series. Here, we use the same approach to investigate the operational use of SAR and optical time series as part of the existing (legacy) forest monitoring scheme. It is thus emphasised that this work does not represent an attempt to build a joint SAR – optical processing system from the ground up. A multi-sensor forest monitoring framework will always face a practical trade-off between the added benefits of supplementary datasets, and the costs associated with the additional processing and expertise required (Furby and Wu, 2009). In this work, we effectively investigate a "low cost" approach to the integration of optical and SAR data by taking advantage of an established and proven monitoring system. Similarly, rather than a direct assessment of accuracy against ground-truth data, the focus here is on an inter-comparison of the optical and SAR results, in order to determine whether potential differences are significant in terms of interoperable forest mapping. This ultimate goal of reproducing optical results is evidently motivated by the fact that NI-LCCP is currently implemented operationally in Australia on the basis of Landsat data. It is therefore important to realise that the SAR results presented here should not necessarily be seen as representative of the forest mapping capacity of SAR sensors in general. The SAR F/NF classifications in this work must be considered in this context of optical reproducibility, i.e., as an outcome resulting from the need to fine-tune the classifier so as to best match the Landsat classifications. It is acknowledged here that the optical nature of the Landsat imagery has motivated some important aspects of Australia's Land Cover Change Program, and the resulting limitations on the use of SAR data within this framework are highlighted and discussed in detail in this paper.

1.2. Existing work

This work builds upon several existing NI-LCCP case studies by the authors on the use of SAR and optical data for forest monitoring (Lehmann et al., 2011, 2012a, 2012b). These earlier studies however focussed on a geographically restricted demonstration site in Tasmania (approx. 2,500 km^2). In contrast, Mitchell et al. (2011a) considered Tasmania-wide forest classifications, with results however obtained independently from Landsat and PALSAR data, and compared in a qualitative manner. Here, we present the latest methodological developments and results obtained in the frame of IFCI's Tasmanian demonstrator program, and add to these earlier case studies in several ways. First, the methods are here generalised both spatially and temporally, thereby demonstrating that the proposed approach remains relevant and robust when applied more broadly to large geographical areas. In particular, this work investigates the use of stratification zones for the implementation of different classification parameters (separation indices and thresholds), which allows for a straightforward use of the methods at continental scales. Also, whereas several of the earlier works cited above focussed on the properties of SAR and optical datasets acquired at a single date, the methodology is here applied so as to achieve temporal consistency, by consideration of the entire time series of SAR data.

Another specific aspect of the current work relates to the consistent treatment of the SAR and optical datasets. In Lehmann et al. (2012a), Mitchell et al. (2011a), the SAR-based F/NF classifications were based on training information different from that used to generate the Landsat-based maps. Compared to the NI-LCCP methods, Mitchell et al. (2011a) also used a different technique for SAR forest classification. Ultimately, these procedural inconsistencies mean that discrepancies between the SAR and optical classifications cannot be linked explicitly to different sensor-related characteristics, leading to a potentially biased interpretation of sensor interoperability. In the present work, a consistent approach is used by applying the standard NI-LCCP processing steps to the SAR imagery, and by making use of training data that lead to the closest possible match with the Landsat-based classifications.

In the following, Section 2 presents an overview of the datasets used in this work, and reviews the characteristics of the study area and associated bioregions. Section 3 presents the methodological details, including a description of the processing steps used within Australia's Land Cover Change Program. The main outcomes from this study are then presented in Section 4, which contains analytical results from: *i)* forest discriminant analyses carried out on the optical and SAR datasets (providing insights into data complementarity); *ii)* comparative assessments of single-date SAR and optical forest classifications; and *iii)* comparative assessments of multi-temporal processing outputs and related change products using two different combinations of the SAR and optical time series (data interoperability). A discussion of these results is finally provided in Section 5, which concludes this paper with some final remarks on operational SAR – optical forest monitoring.

2. Data and study area

2.1. Tasmania: Australia's national demonstrator region

Tasmania, one of several national "demonstrator" regions defined as part of GEO-FCT, is the island state located about 240 km south of the eastern part of the Australian continent (Figure 1). Its land area covers some 68,400 km^2, of which about two thirds are densely forested. As the most mountainous state in Australia, parts of Tasmania exhibit a very rugged topography, culminating at a height of about 1,600 m above sea level. Due to its specific size and location in the Indian and Pacific oceans, Tasmania has a cool temperate climate where temperatures are moderated by the surrounding seas. In comparison to larger land masses at similar latitudes in the northern hemisphere, Tasmania thus exhibits complicated rainfall patterns that can lead to significant extents of cloud cover in Landsat imagery.

As part of the NI-LCCP approach to national forest mapping, the Australian continent is subdivided into a number of stratification zones. On the basis of parameters such as geology, landcover types, and spectral characteristics, these regions were selected so as to locally optimise the reliability and accuracy of the Landsat-based forest classifications. These stratification boundaries are thus not directly relevant to the processing of SAR data, and instead, this work makes use of the more generic biogeographic regions defined by the Australian Government's Interim Biogeographic Regionalisation for Australia (IBRA; Peters and Thackway, 1998). IBRA subdivides Tasmania into nine land bioregions (Figure 1) that represent broad landscape patterns sharing similar environmental, physical and climatic conditions. These bioregions thus provide a good basis for assessing the relevance and need for stratification in the SAR forest classification. As shown in Figure 1 (dashed red lines), the geographical isolation of the north-west and north-east islands allows the further subdivision of the respective stratification zones into northern and southern parts (considered separately in some of the data processing and analyses).

For testing and validation of various processing strategies developed as part of GEO-FCT, three 50 km × 50 km sites were defined in Tasmania: the Takone, Mathinna and Warra sites are shown as black squares in Figure 1. These samples were selected within distinct bioregions for calibration purposes under IFCI, and exhibit different types of forest cover, terrain characteristics and land-use history. The landcover types in these areas include dry and wet native eucalypt forest and woodland, scrub and buttongrass moorland, highland treeless vegetation, as well as rainforest (Harris and Kitchener, 2005), while the main land use types are related to agriculture (crops and pasture) and commercial forestry activities (soft

and hardwood plantations). In the following, these IFCI sites are used as representative geographical samples for targeted analyses of sensor complementarity, while interoperability assessments are based on results obtained for the whole of Tasmania.

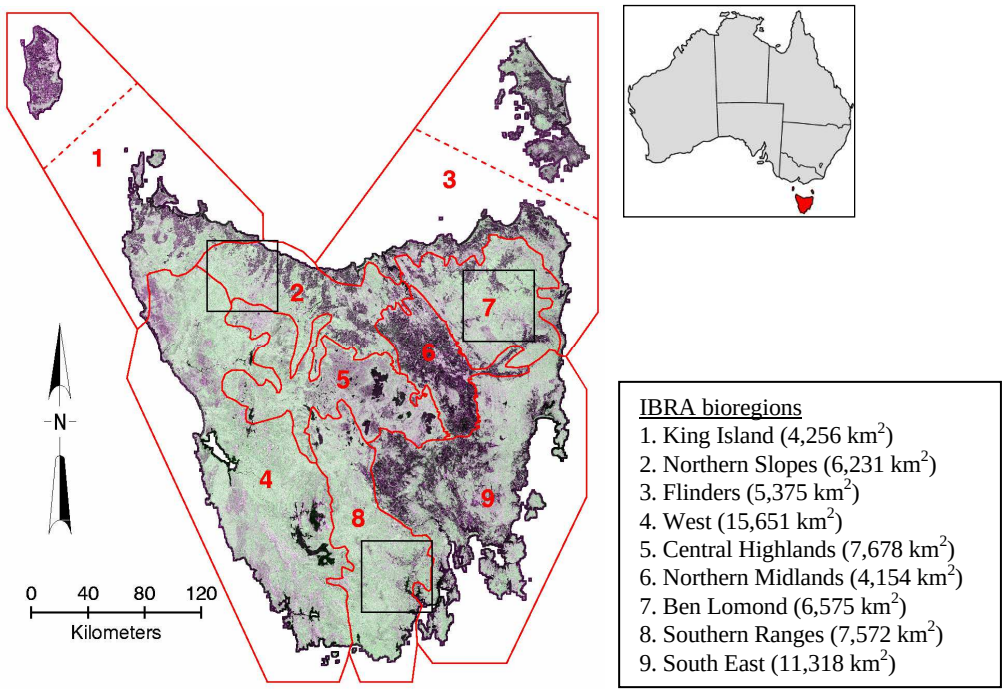

Figure 1. 2007 PALSAR data (HH/HV/HH in R/G/B) with superimposed IBRA stratification zone boundaries and numbering (in red, with corresponding names provided in the legend). The three black squares represent the IFCI calibration sites: Takone in the north-west, Mathinna in the north-east and Warra in the south. *Top-right inset:* map of Australia with Tasmania highlighted in red.

2.2. Datasets

2.2.1. Landsat data

The optical data used in this work was sourced from the existing archive of calibrated and co-registered Landsat MSS/TM/ETM+ imagery over the Australian continent (25 m pixel size) produced as part of NI-LCCP. In Tasmania, the selection of Landsat data typically targets the dry season imagery to minimise cloud affected areas. In order to achieve meaningful landcover change information and minimise various types of errors (geolocation inaccuracies, corrupted pixels, etc.), tight quality standards are imposed during the processing of the Landsat scenes, which includes: ortho-rectification to a common spatial reference, top-of-atmosphere reflectance calibration, calibration to 'like' values (Furby and Campbell, 2001), correction for scene-to-scene differences (using bidirectional reflectance distribution functions), calibration to a common spectral reference (using invariant targets), and correction for differential terrain illumination. Further descriptions and other key aspects of the processing methods are provided in Caccetta et al. (2007), Furby (2002), Furby et al. (2008). From this continental archive, a time series of 19 Landsat mosaics over Tasmania (1972 to 2010) was extracted for use in this work. The extent of cloud-affected areas in this time series is about 26 % on average, ranging from 4 % for the best epoch to 100% for the worst.

2.2.2. ALOS PALSAR data

In the frame of this work, L-band SAR data were available in the form of four existing (fully processed) IFCI mosaics of ALOS PALSAR data (HH and HV, 12.5 m pixel size) over Tasmania, one for each year between 2007 and 2010 (Figure 1). These mosaics were originally generated from individual tiles of fine-beam dual polarisation data (SLC level 1.1, 34.3° off-nadir angle in ascending orbit), acquired between the months of August and October of each year (wet, winter conditions). These scenes were systematically processed to σ^0 (in dB) and composited as described in Mitchell et al. (2011b) and Mitchell et al. (2011a), using a sequence of steps including: multi-looking, speckle filtering (Lee filter), ortho-rectification, radiometric calibration and normalisation, and correction for terrain-induced illumination differences (Zhou et al., 2011). These mosaics are used as input to the complementarity assessments, as well as in the analyses leading

to the selection of forest classification parameters (separation indices and thresholds, Section 3.4.1). The subsequent generation of (single-date) forest maps is based on a segmented version of these PALSAR mosaics, obtained through multi-resolution segmentation applied in Definiens Developer software (Mitchell et al., 2011b).

In addition, specific scenes of raw PALSAR data (SLC level 1.1) covering the three representative calibration sites (described in Section 2.1) were obtained for the present work and re-processed as described above, but excluding the use of speckle filtering. These non-filtered PALSAR data are used for the purpose of deriving texture measures for the complementarity assessments.

2.2.3. RADARSAT-2 dataset

In this work, a forest discrimination analysis using C-band data is carried out for the three IFCI calibration sites. For this purpose, RADARSAT-2 scenes covering these study regions were acquired in September 2009 (wet season), with data acquired in wide-beam (W3) dual-polarisation mode (VV and VH, 42.2° off-nadir angle in ascending orbit). Pre-processing of these SAR images (to 12.5 m pixels) was carried out in a manner similar to that used for the PALSAR data (Section 2.2.2), and a separate dataset of non-filtered RADARSAT data was also produced.

3. Methods

3.1. Data co-registration

An accurate co-registration of the SAR and optical datasets is essential for an integrated (multi-temporal) approach to forest mapping and monitoring. In this work, co-registration assessments were carried out using a digital image correlation (DIC) approach (Sutton et al., 2009), which essentially generalises the feature-matching concept used routinely within NI-LCCP (gradient cross-correlation; Campbell and Wu, 2008) to large spatial extents. Here, we use Pearson's product-moment correlation coefficient r_{xy}, computed on the basis of the SAR and optical pixel intensities x_i and y_i, respectively, for $i = 1, \dots, N$ image pixels:

$$r_{xy} = \frac{\sum_{i=1}^{N}(x_i - \bar{x})(y_i - \bar{y})}{\sqrt{\sum_{i=1}^{N}(x_i - \bar{x})^2 \cdot \sum_{i=1}^{N}(y_i - \bar{y})^2}} \quad (1)$$

where $\bar{x}$ and $\bar{y}$ represent averages over the respective regions. Maximising r_{xy} over a range of horizontal and vertical shifts of one image with respect to the other identifies the displacement existing between the datasets. It thus also provides the correction to apply to one of the datasets so as to achieve the best data co-registration. In this work, we used TM band 5 for Landsat and the cross-polarised SAR data for the computation of the coefficient r_{xy}.

The DIC approach can be applied to entire images or smaller sub-areas. Here, we applied it separately to each stratification zone in each year so as to provide more localised co-registration assessments. The Landsat imagery was used as a reference due to the PALSAR data being available at a resolution of 12.5 m, thereby allowing for a finer adjustment of co-registration without the need for data re-sampling. Results show that in all zones except for the northern part of Zone 3, the maximum shift between the PALSAR and Landsat data is 2.2 SAR pixels (12.5 m pixel size), corresponding to one pixel shift in one direction (horizontal or vertical) and two in the other. On average, PALSAR is co-registered with Landsat to less than one optical pixel (25 m). Given the independent processing of these datasets, this represents a result that compares well with a similar assessment of geolocation accuracy carried out in Shimada and Ohtaki (2010). The exception here is the northern part of Zone 3, where the two datasets have displacements ranging between 5.0 and 7.8 SAR pixels.

A similar analysis was carried out for the RADARSAT data with respect to the 2009 Landsat image over the three IFCI calibration sites, with results similar to those described above for PALSAR. As a coarse rectification measure prior to data processing, these results were used to correct the SAR data within each stratification zone or IFCI site, thus leading to an overall registration accuracy of less than one Landsat pixel. Such a level of accuracy was deemed sufficient for the analyses and methods described in this work.

3.2. Texture measures

This work also investigates the use of SAR-based texture information as input to the F/NF classifications. Various methods exist for deriving texture information (e.g., Zhang and Tan, 2002), and we considered a number of typical measures computed using standard first and second-order local statistics (Kuplich et al., 2005; Zhang, 2001), as well as grey level co-occurrence matrix (GLCM) measurements (Haralick et al., 1973). Local statistics (LS) describe the moments of a neighbourhood of individual pixels in a given image region, while GLCM-based texture measures characterise the distance and angular relationships among pixels. This work assessed a total of 18 different texture measures relating to the degree of disorder, similarity (uniformity) and central tendency among image pixels, namely:

- GLCM variance, correlation, contrast, dissimilarity, homogeneity, entropy, angular second moment, maximum probability, and chi squared measure; and
- LS contrast, energy, entropy, homogeneity, variance, mean absolute deviation, coefficient of variation, skewness, and kurtosis.

These measures were computed for both SAR polarisations and for three different window sizes each (5, 9 and 13-by-13 pixels). The GLCM texture parameters were calculated for all eight directions (omni-directional) on the basis of a uniform quantisation into 64 grey levels. The non-filtered PALSAR and RADARSAT data (12.5 m pixel resolution) were used when computing these texture parameters (Sections 2.2.2 and 2.2.3).

3.3. Canonical variate analysis

Analyses of forest discrimination, as well as F/NF classifications within NI-LCCP strongly rely on a linear discriminant technique called canonical variate analysis (CVA; Campbell, 1994). Given a set of training sites, this method is used to find uncorrelated linear combinations of image bands (canonical vectors, CVs) providing the best separation between the forest and non-forest classes. At each training site, only the mean value in each image band is considered; CVA thus does not assume any specific distribution of the input data. Canonical vectors are determined by maximising the ratio μ of between-class to within-class variability among the training data:

$$\boldsymbol{v}^* = \arg\max_{\boldsymbol{v}}(\mu) = \arg\max_{\boldsymbol{v}}\left(\frac{\boldsymbol{v}^T\boldsymbol{B}\boldsymbol{v}}{\boldsymbol{v}^T\boldsymbol{W}\boldsymbol{v}}\right) \quad (2)$$

where $\boldsymbol{B}$ represents the training sites' between-class variation matrix, and $\boldsymbol{W}$ is the sites' within-class variation matrix. This process can be seen as projecting the sites from each class onto a line (in the multi-dimensional data space) such that the variance of the means of each class on the line is as large as possible relative to the average variance of the observations within each class. Once the first CV is found (direction of maximum discrimination among the training sites), successive CVs are determined in turn in a similar manner subject to being orthogonal (uncorrelated) to previous ones.

In Eq. (2), the variable μ is known as the canonical root (for a given CV) and characterises the magnitude of the between-class variation along the direction of maximum separability defined by $\boldsymbol{v}^*$. It represents a normalised separation metric that provides a quantitative indication of discrimination, and can be used to compare the characteristics of different datasets in terms of F/NF classification. In particular, the ratio of two canonical roots (e.g., obtained with two different datasets) can be used as a measure of improvement in forest discrimination of one dataset over the other. This essentially forms the basis for the variable selection method of MacKay and Campbell (1982), which is used here to provide assessments of complementarity between the SAR and optical datasets. CVA can also be used as a data reduction method for display purposes to further investigate forest discrimination, and for the selection of separation indices for F/NF classification (Furby, 2002). More details on CVA can be found in Campbell (1994), Lehmann et al. (2012a).

3.4. Data processing workflow within existing (legacy) system

3.4.1. Main processing steps

The main focus of Australia's Land Cover Change Program was the development of reliable operational methods for a temporally consistent mapping of forested regions at continental scale. Aspects such as accuracy, spatial and temporal reliability, computational efficiency, and interpretability were thus considered critical in the methodological developments. The resulting data processing workflow includes the following key steps (Furby, 2002):

1. Definition of a forest classifier, for each stratification zone, according to:
    a. selection of two to four images representative of the multi-temporal sequence,
    b. selection of training sites representative of the various forest and non-forest covers,
    c. using CVA, calculation of two (or more) spectral indices to discriminate between the forest and non-forest classes,
    d. simplification (smoothing) of these indices to ensure a reliable and consistent applicability to all epochs in the time series.
2. In each stratification zone and for each epoch in the time series, calculation of forest cover probabilities by selecting, for each spectral index, thresholds identifying the (soft) boundaries between the forest and non-forest classes; this is achieved through a matching process (Caccetta et al., 2007) using a base probability image as reference data (as well as manual fine-tuning where necessary).
3. Creation of "single-date" forest probability maps for all epochs through aggregation of the zone-based F/NF classification results into wide-area mosaics.
4. Refinement of the single-date probability images using a spatio-temporal model for forest classification (conditional probability network).

5. Production of final change maps and other aggregated products.

This framework is generic in nature, and while originally developed on the basis of Landsat data, it allows for the multi-temporal integration (in Step 4) of data from any time series of co-registered and calibrated remote sensing imagery (Caccetta, 1997; Furby and Wu, 2009). The above processing steps are here applied rigorously to the SAR data for integration within this existing framework, thereby allowing for an assessment of SAR – optical interoperability.

3.4.2. Discussion

As stated in Section 1.1, the aim of this work is to determine to which extent SAR data can be used to reproduce the existing (Landsat-based) NI-LCCP results. The use of independent SAR training data would thus preclude a direct comparison with optical results. Consequently, the F/NF training sites for the SAR classifications (Step 1.b) are here selected on the basis of the Landsat-based forest maps themselves. For each year, approximately 400 training sites (169 pixels each, 12.5 m resolution) are selected randomly within each stratification zone according to the main landcover classes, and labelled according to the corresponding single-date Landsat F/NF classification. This training dataset is then used for the computation of the SAR-based classifications in Steps 1.c and 1.d above. While acknowledging that it does not represent accurate ground truth information, this selection of the SAR training data represents the most relevant option when attempting to match the Landsat results. Note also that this selection process may result in sub-optimal SAR classifications due to the forest labels not necessarily accounting for the (complementary) characteristics of the SAR data.

The selection of (soft) thresholds in Step 2 typically relies on a base probability image generated for the entire Australian continent using the 1998 Landsat data. In regions such as Tasmania, however, classification difficulties arise due to frequent and widespread cloud cover. It is thus not unusual for the matching process to rely on the previous year's F/NF results instead, so as to improve the reliability of the estimated index thresholds. In this work, we use the 2006 NI-LCCP forest map as a matching base image for the SAR classifier, though it is stressed that the use of different matching data does not ultimately lead to significant differences in forest classification.

It should also be mentioned that the approach used here for the generation of single-date maps of forest probabilities (Steps 1 to 3) is very similar to the methods used to produce JAXA's PALSAR-based worldwide F/NF maps. As described by Shimada et al. (2014), these maps are essentially generated through a thresholding of segmented HV mosaics.

The spatio-temporal model used in Step 4 improves the mapping accuracy and temporal consistency of the forest classifications by reducing false transitions between classes (noise) and by inferring the label of missing pixels (e.g. cloud-affected) using all available spatial and temporal data (Caccetta, 1997; Caccetta et al., 2010). Based on a Bayesian conditional probability network (CPN), it essentially provides a framework for the assessment and propagation of uncertainty in the classification of data with varying levels of quality and accuracy (Caccetta et al., 2007; Kiiveri et al., 2003). This framework is here implemented as a first-order hidden Markov model that represents the spatial and temporal relationships between the image data $\boldsymbol{x}_{k,m}$ (for the k-th pixel and m-th epoch), the unobserved "true" class labels $\ell'_{k,m}$ and the corresponding classification labels $\ell_{k,m}$ estimated by the single-date classifier. For the k-th image pixel, this model can be represented mathematically as follows:

$$p\left(\boldsymbol{x}_{k,1}, \dots, \boldsymbol{x}_{k,M}, \ell_{k,1}, \dots, \ell_{k,M}, \ell'_{k,1}, \dots, \ell'_{k,M}, R_k\right) = \prod_{m=1}^{M} Q_1 \cdot Q_2 \cdot Q_3 \cdot Q_4 \tag{3}$$

where R_k denotes the group of pixels spatially adjacent to pixel k (8-pixel neighbourhood). In this formulation, $Q_1 = p\left(\boldsymbol{x}_{k,m} \middle| \ell_{k,m}\right)$ essentially corresponds to the single-date forest probabilities (likelihood of the estimated class given the data), $Q_2 = p\left(\ell_{k,m} \middle| \ell'_{k,m}\right)$ represents the error rates of the estimated landcover class given the true labels (sensor bias), and $Q_3 = p\left(\ell'_{k,m} \middle| \ell'_{k,m-1}\right)$ specifies the temporal rules indicating the likelihood of transitions between classes from one epoch to the next. In practice, Q_2 and Q_3 are typically represented as contingency tables specified or estimated from the available data (Furby et al., 2008). $Q_4 = p\left(\ell'_{k,m} \middle| R_k\right)$ is a spatial term that influences the pixel's class according to the dominant neighbourhood label, and is defined as $Q_4 \propto \exp\left(c_k\right)$ where c_k is the number of pixels in R_k having the same label as pixel k (Caccetta, 1997). Fitting this model to the data allows the computation of $p(\ell'_{k,m} | \boldsymbol{x}_{k,m})$, i.e., the probability of the unobserved "true" class label given the multi-temporal data. The output from this model is thus also in the form of probability images, where the forest probabilities have been refined by the temporal and spatial rules, while accounting for the error rates defined within the model.

In Step 5, forest change products are finally generated by simple differencing (subtraction) of the class labels between two time steps of interest, so as to achieve a change map indicating deforestation, afforestation and 'no change' pixels. Note that in general, the subtraction of two thematic maps obtained from single-date classifications is undesirable for change detection since the mapping inaccuracies in both maps compound, leading to an increased uncertainty in the post-classification change product (Congalton and Green, 2009). However, the multi-temporal approach used here is not affected by this issue as it essentially provides estimates of the underlying F/NF state for each pixel using the model's spatial and temporal rules. In particular, it can be seen that the estimated forest probabilities rely on the entire time series

of image data. In contrast to a comparison based on pairs of classified (single-date) images, the current approach thus allows for robust change detection from two different state estimates.

3.5. Evaluation of change maps

Tasmania-wide classifications obtained from different sensors can be compared by overlaying one classification on another, cross-tabulating the results in a confusion matrix, and calculating statistics such as the *kappa* coefficient, user's and producer's accuracy, and so on (Congalton and Green, 2009). While this approach provides a useful overall evaluation as a global census of the area of interest, it does not allow testing for significant differences among classifications, nor does it facilitate comparisons at different spatial scales. In addition, it does not reflect the way that sample-based operational evaluations are usually undertaken.

To provide additional insight at global, regional, and local scales, a number of area-based samples can be extracted from the maps and analysed in a variety of ways. By nature, carbon accounting relies on the accurate detection of changes in forest extents between two epochs of interest. In this work, this area-based approach is used specifically to quantify the significance of differences in change maps obtained on the basis of the Landsat and SAR time series.

For each areal sample, the amounts of each change class (i.e., deforestation, afforestation, and 'no change') are extracted from the maps under comparison, and analysed using three different metrics addressing different spatial scales. First, 95 % confidence limits are calculated for each landcover change type on the map being evaluated, and compared to the corresponding amounts calculated from the whole of the reference map. This addresses interoperability at a global (whole-of-Tasmania) spatial scale. The second metric is an "areal confusion matrix," where data from the areal samples are tabulated against the reference data with respect to the entire sample unit; results for all sample units are then tabulated into a single confusion matrix. In this approach, an areal sample with the same extents of landcover change in both maps is considered completely correct, even if the exact locations of the change classes within a given areal sample are not identical (Pontius and Cheuk, 2006). This approach addresses interoperability at a "regional" scale (i.e., at the scale of the areal sample). The third metric is a conventional pixel-by-pixel confusion matrix of map data against reference data, computed over all pixels in the areal samples, which addresses interoperability at a local scale. Note that intra-sample locational differences will impact the pixel-based confusion matrix, whereas the areal confusion matrix effectively relaxes the requirement of individual pixel agreement.

4. Results

4.1. Assessment of SAR – optical complementarity

To assess the degree of forest discrimination typically provided by the optical and SAR data, a discriminant analysis was carried out at each of the three IFCI calibration sites, using 2009 data. To this purpose, the PALSAR and RADARSAT data were re-sampled to 25 m pixels (2-by-2 averaging) so as to match the resolution of the Landsat data. The results below were obtained on the basis of approximately 275 F/NF training sites (121 pixels each) selected randomly from the main landcover classes in each calibration site. Sites from the forest group were then contrasted against the non-forest group using CVA. Discriminant information (Table 1) was extracted by comparison (ratio) of the canonical roots obtained with subsets of the available data against that resulting from using all available SAR and optical data simultaneously (variable selection; see MacKay and Campbell, 1982).

For information, Table 1 also includes the Jeffreys–Matusita (JM) distance, which provides a different measure of statistical separability between two distributions (Canty, 2014); this metric is asymptotic in $\sqrt{2}$, with this upper bound suggesting complete separability and 0 indicating inseparable classes. Although the JM distance is widely used in practice, CVA is here used as a basis for both the variable selection process and the subsequent selection of F/NF classification indices; the variable selection results in Table 1 can thus be expected to provide more relevant information in the frame of this work.

The results are consistent across the three calibration sites, and reveal several characteristics of the datasets when used for the purpose of forest discrimination. As shown in Table 1 on Lines 2 and 5, the cross-polarised data are best at separating the forest and non-forest sites for both the L-band and C-band SAR data, with the co-polarised band adding little more to this separability (Lines 3 and 6). Similarly, a comparison of Line 3 with Line 7 shows that the addition of RADARSAT to PALSAR only provides a limited overall gain in terms of forest discrimination (i.e. limited additional or complementary information). The combination of Landsat and PALSAR can be seen to achieve most of the discrimination (Line 13), and compared to the individual datasets' discriminative properties (Lines 3 and 11), this result demonstrates a significant complementarity between these SAR and optical data. The addition of RADARSAT somewhat improves the discrimination of the Landsat-only results (Line 12 vs. Line 11); with Sentinel-1 data to become available free of charge to public users soon (and while ALOS-2 data are limited to commercial provision), this result indicates that single-date C-band data can provide some small but significant improvement in addition to Landsat in case L-band SAR data cannot be afforded. Table 1 however indicates that the RADARSAT data does not lead to a significant improvement in conjunction with the combined Landsat and PALSAR datasets (Line 13 vs. Line 14).

Table 1. Discriminant analysis results (with JM distance in parentheses) for the Landsat, PALSAR and RADARSAT data in 2009, at each of the three IFCI calibration sites. Values indicate the degree of forest discrimination achieved by various combinations of SAR and optical bands, as a percentage of the total discrimination achievable using all datasets simultaneously.

	image bands		percentage discrimination (JM distance)		
			Mathinna	Takone	Warra
1	PALSAR	HH	22.2 % (0.979)	19.7 % (0.927)	21.1 % (0.970)
2		HV	66.0 % (1.086)	49.9 % (1.019)	60.4 % (1.040)
3		HH + HV	66.6 % (1.230)	50.3 % (1.191)	60.9 % (1.265)
4	RADARSAT	VV	4.8 % (0.611)	2.0 % (0.763)	5.0 % (0.813)
5		VH	14.0 % (0.882)	5.7 % (0.770)	12.5 % (0.855)
6		VV + VH	14.8 % (1.164)	5.8 % (1.113)	12.9 % (1.152)
7	PALSAR + RADARSAT		68.4 % (1.351)	50.9 % (1.335)	62.2 % (1.357)
8	Landsat TM	best band	B5: 54.0 % (0.784)	B5: 71.2 % (0.870)	B5: 42.4 % (0.815)
9		best 2 bands	B4, B5: 59.5 % (1.110)	B5, B6: 74.1 % (1.197)	B1, B5: 47.3 % (1.196)
10		best 4 bands	B2, B4, B5, B6: 60.3 % (1.342)	B3, B4, B5, B6: 76.8 % (1.348)	B1, B4, B5, B6: 56.1 % (1.358)
11		all bands	61.0 % (1.387)	76.8 % (1.396)	58.2 % (1.399)
12	Landsat TM + RADARSAT		72.9 % (1.407)	80.7 % (1.409)	69.5 % (1.411)
13	Landsat TM + PALSAR		97.4 % (1.408)	99.9 % (1.410)	98.3 % (1.412)
14	TM + PALSAR + RADARSAT		100.0 % (1.412)	100.0 % (1.413)	100.0 % (1.413)

These results provide quantitative information related to the complementarity of the optical and SAR datasets for forest mapping, thereby highlighting the potential advantages of using SAR-based information in the context of a forest monitoring system. It must be noted that different results would likely be obtained if the analyses were carried out using multiple classes of landcover types (e.g. plantations, forest species, urban areas, etc.). Due to the limited additional benefits of the single-date C-band SAR data in the present forest mapping context, however, the RADARSAT dataset was deemed redundant and the interoperability assessments (Section 4.3 onwards) are thus based on the use of L-band PALSAR data only.

4.2. Discriminant analysis with SAR texture

Variable selection analyses (same approach as in Section 4.1) were carried out to investigate the use of SAR-based texture information at each of the three representative IFCI sites. This led to the identification of the texture measures (sometimes differing across sites) providing the best improvement of discrimination on top of the SAR and Landsat bands. For PALSAR, the LS HV coefficient of variation, together with the GLCM HV entropy, both of them computed for a window size of 13-by-13 pixels, were found to improve the discrimination most, with an average increase of 18.5 %. For RADARSAT, the LS coefficient of variation for VV and VH (13-by-13-pixel window) were best, though only achieving an average increase of about 5.8 %.

Further analyses were carried out to determine the overall improvement in classification accuracy achieved by the addition of these texture measures to the SAR data alone. A marginal improvement of at most 1.7 % (Warra site in 2007) resulted for PALSAR, while the addition of textural parameters to the RADARSAT data was not found to increase the accuracy noticeably. These results indicate that texture did not specifically increase the separability of the forest and non-forest sites located at the boundary between the two classes (within the “uncertain” region). A visual assessment also confirmed that the use of texture did not improve the classifications in areas where typical SAR mapping errors occur (such as recently harvested plantations, for instance). The addition of texture bands thus did not translate into significant improvements in classification accuracy compared to the use of the SAR data alone.

This outcome can be explained by the fact that the variable selection and classification accuracy analyses are here concerned with only two broad classes of interest (forest/non-forest). Texture has proved useful in many case studies involving multi-class approaches to landcover classification (e.g. Longépé et al., 2011; Otukei et al., 2011; Vaglio Laurin et al., 2013), where texture information has been shown to significantly improve the classification in specific areas such as urban regions, mature plantations, complex forests, etc. Due to the large-scale focus of this work, however, such areas remain geographically limited in comparison to the overall extents of forested and non-forest regions. In keeping with Longépé et al. (2011), it can thus be argued that the contribution of textural parameters to the F/NF classification is here restricted, with any associated gain in classification accuracy to be considered in the context of the additional processing load resulting from the introduction of texture information in a large-scale operational setting.

4.3. Single-date classifications

4.3.1. PALSAR processing

This section provides the F/NF classification results obtained by applying the processing methods described in Section 3.4 to the PALSAR data. The 12.5 m resolution of the PALSAR data was kept throughout the processing sequence until the thresholding process (Step 2 in Section 3.4), where the single-date forest probability maps are generated at 25 m pixel size by simple averaging of four 12.5m pixels. Also, while the spatio-temporal model described in Section 3.4.2 already contains a spatial component, segmentation of the PALSAR data was used as a further speckle rejection measure and to improve spatial homogeneity. The original (non-segmented) mosaics were used for the selection of classification indices and thresholds, while the final thresholding process (leading to the single-date maps of forest probabilities) was applied to the segmented PALSAR mosaics.

Although the emphasis here is on forest cover, it is important to ensure that the full range of landcover types is represented in the set of SAR training sites. These were thus selected by considering the different clusters in the HH – HV data space (essentially representing different landcover types), leading to a training dataset providing a roughly complete representation of the data. As discussed in Section 3.4.2, these sites were subsequently labelled as forest or non-forest on the basis of the single-date Landsat classifications, in an attempt to reproduce the NI-LCCP results.

To assess the need for stratified classification of the SAR data, the classification was applied to each stratification zone separately. Table 2 presents some of the results, including the selected (smoothed) classification indices and the selected soft thresholds (achieved through a matching process with respect to the base probability image, see Step 2 in Section 3.4.1). These thresholds indicate the boundaries of the "uncertain" region contained between the "certain" forest and non-forest regions, and are used to assign forest probabilities to each image pixel. For instance, for a given pixel k in Zone 1 in 2007, the forest probability (in %) results as follows:

$$Q_{1,k} = \begin{cases} 100.0 & \text{if } \left(I_{1,k} \le 105.0\right) \text{ and } \left(I_{2,k} \ge -119.0\right) \\ 0.0 & \text{if } \left(I_{1,k} \ge 124.0\right) \text{ or } \left(I_{2,k} \le -133.0\right) \\ 100.0 \cdot \min\left\{\dfrac{I_{1,k} - 124.0}{105.0 - 124.0}, \dfrac{I_{2,k} + 133.0}{133.0 - 119.0}\right\} & \text{otherwise} \end{cases} \tag{4}$$

$$I_{1,k} = 4 \cdot \mathrm{HH}_k - 9 \cdot \mathrm{HV}_k \tag{5}$$

$$I_{2,k} = 6 \cdot \mathrm{HH}_k + 4 \cdot \mathrm{HV}_k \tag{6}$$

where HH_k and HV_k (in dB) represent the pixel's co- and cross-polarised SAR values, respectively.

The smoothed indices in Table 2 all achieve an average discrimination level (over four years) of at least 96.3 % compared to the original (non-smoothed) CVA coefficients. For all zones, the first index essentially represents a "contrasting" index, built by subtraction of the HV band from the HH band (or multiples thereof), while the second index represents an "intensity" index (addition of the two polarisations). However, these classification indices can be very different across stratification zones, due to different vegetation covers, land-use types and soil characteristics. Also, the selected classification thresholds vary significantly across years, as well as spatially across those zones with identical indices (Index 1 for Zones 2 and 3; Index 2 for Zones 6, 8 and 9). These spatial and temporal variations mean that the use of stratification is relevant for improved forest classification over large geographical extents such as Tasmania.

This result is of particular interest in light of initiatives such as JAXA's worldwide F/NF map, achieved through thresholding of HV data from a global PALSAR mosaic. Shimada et al. (2014) also recognised the need for region-specific thresholds in the development of this product. However, these thresholds were defined as being constant over the 2007 – 2010 period, and were stratified according to 15 large (continental-scale) regions. In that work, for instance, the PALSAR classification thresholds for continental Australia were determined based on a total of 11 areal samples of F/NF cover (40 to 50 km^2 each).

Finally, single-date forest probability images for the PALSAR data were generated by aggregating the zone-based classification results (obtained via thresholding of the SAR data as per Table 2) into a single mosaic for each year. Figure 2 shows an example of the PALSAR forest map for 2007 (left) together with the corresponding Landsat-based NI-LCCP classification (right).

Table 2. Separation indices and thresholds selected for PALSAR forest classification in each biogeographic zone. The 'Index' columns provide the multiplicative coefficients of the HH and HV bands for the respective index (smoothed coefficients). The 'thresholds' columns contain the selected classification thresholds for each year and each index, determining the limits of the 0 % and 100 % forest regions.

Zone	Index 1	Index 2		thresholds (dB)			
				2007	2008	2009	2010
1	(4, -9)	(6, 4)	Index 1	(105.0, 124.0)	(103.0, 118.0)	(95.0, 118.0)	(96.0, 117.0)
			Index 2	(-133.0, -119.0)	(-139.0, -124.0)	(-143.0, -116.0)	(-150.0, -115.0)
2	(4, -8)	(1, 6)	Index 1	(92.0, 100.0)	(87.0, 99.0)	(85.0, 96.0)	(85.0, 96.0)
			Index 2	(-108.0, -99.0)	(-104.0, -96.0)	(-104.0, -96.0)	(-106.0, -97.0)
3	(4, -8)	(7, 1)	Index 1	(109.0, 125.0)	(103.1, 119.2)	(104.0, 114.0)	(98.0, 115.0)
			Index 2	(-120.0, -103.0)	(-115.0, -92.5)	(-105.0, -95.0)	(-110.0, -94.0)
4	(6, -5)	(2, 6)	Index 1	(26.0, 40.0)	(25.0, 34.0)	(23.0, 31.0)	(26.0, 35.0)
			Index 2	(-125.0, -114.0)	(-117.0, -108.0)	(-122.0, -109.0)	(-122.0, -110.0)
5	(5, -5)	(7, 2)	Index 1	(47.0, 55.0)	(43.0, 75.0)	(42.0, 54.0)	(43.0, 70.0)
			Index 2	(-133.0, -108.0)	(-150.0, -100.0)	(-128.0, -100.0)	(-150.0, -112.0)
6	(2, -8)	(6, 3)	Index 1	(117.0, 135.0)	(117.0, 130.0)	(120.3, 141.2)	(112.0, 125.0)
			Index 2	(-116.0, -102.0)	(-120.0, -105.0)	(-115.9, -92.6)	(-114.0, -103.0)
7	(3, -10)	(5, 4)	Index 1	(140.0, 148.0)	(138.0, 153.0)	(130.0, 140.0)	(130.0, 145.0)
			Index 2	(-127.0, -125.0)	(-122.0, -120.0)	(-116.0, -114.0)	(-119.0, -116.0)
8	(5, -7)	(6, 3)	Index 1	(60.0, 90.0)	(57.0, 85.0)	(63.0, 80.0)	(60.0, 80.0)
			Index 2	(-137.0, -123.0)	(-127.0, -112.0)	(-130.0, -115.0)	(-145.0, -130.0)
9	(3, -7)	(6, 3)	Index 1	(95.0, 110.0)	(94.0, 110.0)	(88.0, 105.0)	(90.0, 107.0)
			Index 2	(-123.0, -110.0)	(-124.0, -108.0)	(-113.0, -101.0)	(-122.0, -106.0)

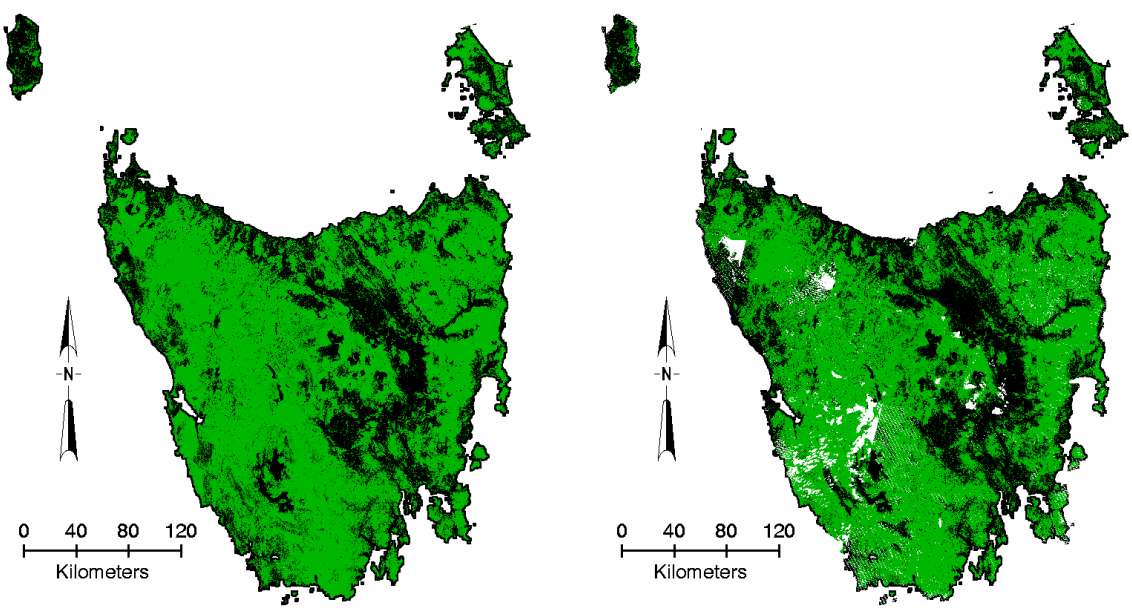

Figure 2. F/NF classifications achieved with the PALSAR data (left) and Landsat data (right) for 2007, with forest probabilities shown in shades of green. In the Landsat image, white pixels are masked due to clouds and sensor deficiencies.

4.3.2. Comparison with optical classifications

For an assessment of SAR interoperability with optical results, these Tasmania-wide PALSAR-based forest maps were compared to the corresponding single-date Landsat classifications. For each year, Table 3 shows the (pixel-based) confusion matrices of resulting forest and non-forest areas in the optical and SAR classifications; the use of PALSAR as the dataset being "evaluated" is here purely arbitrary and does not alter the comparison results in any sense. Invalid pixels

(e.g., due to cloud cover in Landsat) were excluded from the analysis, which explains the different total areas processed in each year. This table also includes the *kappa* coefficient of agreement between the two datasets (Cohen, 1960), which represents the difference between actual agreement and the agreement expected by chance alone. As shown by the *kappa* values and by a consistent mapping accuracy of about 87.2 %, these results indicate a good agreement of Tasmania-wide F/NF extents between the Landsat and PALSAR results (with an average bias of about 5.4 % towards more forested areas for PALSAR).

Table 3. F/NF confusion matrices between the Tasmania-wide single-date PALSAR and Landsat classification maps. All area-related values are given in km^2. The percentage value given next to the total PALSAR forest amount indicates the difference compared to the Landsat results, relative to the total processed area. The 'acc. total' column shows the total accuracy as the percentage of pixels in agreement between the Landsat and PALSAR maps, while 'comm. error' and 'omiss. error' entries correspond to commission and omission error, respectively. All *kappa* coefficients in the last column are statistically significant ($p < 0.001$).

		PALSAR F	PALSAR NF	area total	comm. error	acc. total	*kappa* coeff.
2007	Landsat F	41,387.0	2,604.4	43,991.4	5.9 %	87.5 %	0.706
	Landsat NF	5,627.6	16,013.0	21,640.6	26.0 %		
	area total	47,014.6 (+4.6 %)	18,617.4	65,632.0			
	omiss. error	12.0 %	14.0 %				
2008	Landsat F	36,839.0	1,958.7	38,797.8	5.0 %	87.8 %	0.710
	Landsat NF	5,020.3	13,596.2	18,616.5	27.0 %		
	area total	41,859.3 (+5.3 %)	15,554.9	57,414.2			
	omiss. error	12.0 %	12.6 %				
2009	Landsat F	30,515.9	2,221.2	32,737.1	6.8 %	86.8 %	0.708
	Landsat NF	4,603.9	14,323.5	18,927.4	24.3 %		
	area total	35,119.8 (+4.6 %)	16,544.7	51,664.5			
	omiss. error	13.1 %	13.4 %				
2010	Landsat F	35,165.5	1,888.4	37,053.9	5.1 %	86.5 %	0.695
	Landsat NF	5,904.7	14,913.3	20,818.0	28.4 %		
	area total	41,070.2 (+6.9 %)	16,801.6	57,871.9			
	omiss. error	14.4 %	11.2 %				

For insight, Table 4 provides the mapping accuracy of the single-date F/NF classifications compared to the base probability image (used during the matching process) and to the TASVEG dataset, a state-wide vegetation map from the Department of Primary Industries, Parks, Water, and Environment (DPIPWE, 2009; Harris and Kitchener, 2005). Released in 2009, TASVEG represents a mapping of approximately 154 distinct vegetation communities in Tasmania and is typically used for a broad range of natural resource management and reporting applications. Like any map of this kind, it has its own sources of error which must be kept in mind when using it as reference. In particular, the TASVEG data was collected over a 10 year period in various parts of Tasmania, which would thus preclude its use for accuracy assessment at any single point in time. However, under the reasonable assumption that the vast majority of the ground cover in Tasmania remains consistent with TASVEG over time, we use this information for broad comparison purposes of the SAR and optical F/NF classifications. For completeness, Table 4 also includes the comparison results for the Landsat forest probability maps.

Table 4. Forest mapping accuracy (pixel-based) of the single-date Landsat and PALSAR classifications against the base probability image and the TASVEG dataset. For this comparison, all forest probability images were thresholded at the 50 % level.

year	PALSAR F/NF classification accuracy		Landsat F/NF classification accuracy	
	vs. base	vs. TASVEG	vs. base	vs. TASVEG
2007	85.8 %	80.3 %	90.4 %	78.7 %
2008	85.3 %	80.9 %	89.3 %	81.0 %
2009	85.0 %	80.9 %	88.3 %	79.5 %
2010	85.2 %	80.2 %	89.1 %	80.1 %

Both datasets can be seen to achieve similar levels of accuracy compared to TASVEG. However, the Landsat classifications consistently exhibit an improvement of about 4.0 % compared to PALSAR when assessing the accuracy against the base image. Not surprisingly, this reflects the improved ability of Landsat to consistently reproduce the local and other specific features of the reference image (also Landsat-based). While the PALSAR classifications provide a good representation of the main F/NF extents, some regions with specific landcover types prove difficult to identify correctly with the PALSAR data alone using the current methods, leading to the overall decrease in mapping accuracy compared to the Landsat data.

An example of such mapping differences is provided in Figure 3, which shows a region of native dry eucalypt forest affected by a clearing event in 2009. As shown in this example, this event can be clearly mapped with the Landsat data. It however leads to more subtle and ambiguous PALSAR changes that are more difficult to separate from the surrounding forested areas, thereby leading to a less clear-cut SAR classification. Similar differences can be found in many other regions of plantations and forestry activities. Depending on the local harvesting practices, various debris, logs and branches are left on the ground following a clear-fell, thereby generating strong cross-polarised SAR returns (volume scattering) and limiting the ability of L-band SAR to discriminate between a mature and recently harvested plantation (Shimada et al., 2014). Similarly, the PALSAR data might identify re-planted areas as forest earlier than Landsat due to the presence of medium-size seedlings that might not yet be visible optically.

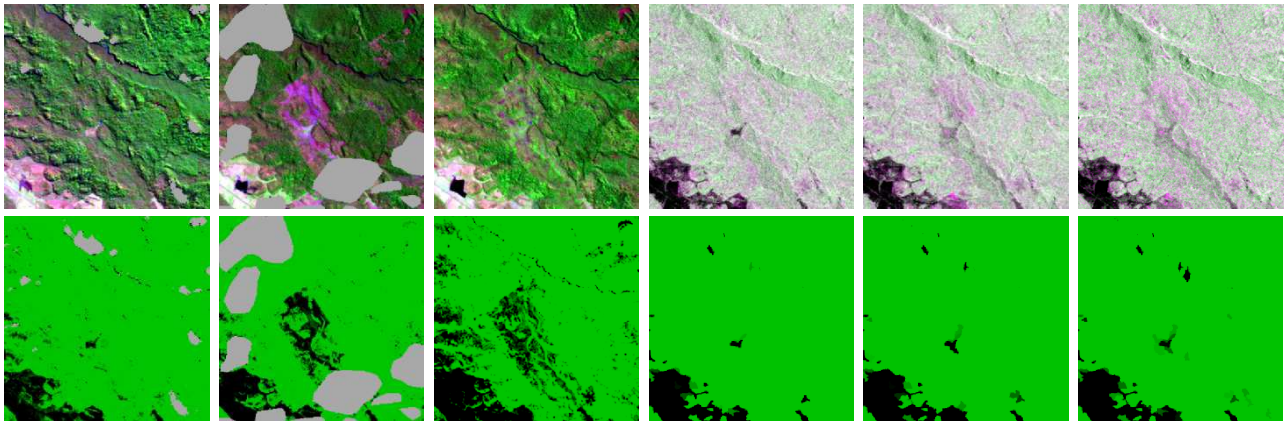

Figure 3. Example of F/NF classifications in a 6.5 km × 6.5 km area located in the Mathinna site. The six images on the left show the Landsat data (top row, bands 5/4/2 in R/G/B) and classifications (bottom row, forest probabilities in shades of green) for 2007, 2009 and 2010. The corresponding PALSAR data (HH/HV/HH in R/G/B) and classifications are given on the right. Grey regions in the Landsat data and classifications correspond to masked (cloud-affected) pixels.

From a visual inspection of the classification results, other areas where similar thematic differences typically occur include the following cases.

- Areas of dense urban development (towns and cities), which exhibit PALSAR signatures very similar to forested regions, thus leading to confusion in the PALSAR classifications.
- Fire scars, which are more likely to appear as non-forest in the Landsat classifications following the fire event while being more difficult to detect in the PALSAR imagery.
- Regions of specific vegetation types, such as buttongrass moorland, sedgeland and highland scrub, which are correctly classified as non-forest with PALSAR but lead to confusion in the Landsat classifications.

Despite similar classifications achieved by the optical and SAR data (Table 3), differences of this kind, together with the difficulties in using PALSAR to reproduce the existing base image (Table 4), point to practical impediments to a full interoperability of optical and SAR data in the context of the existing forest monitoring scheme.

4.4. Assessment of multi-temporal sensor interoperability

The second objective of this work is related to the assessment of interoperability between SAR and optical datasets. This section provides the results from the multi-temporal processing of the PALSAR and Landsat time series, carried out by means of the spatio-temporal model (Section 3.4). Due to the short time series of PALSAR images used in this work (2007 – 2010), all four years were considered in parallel when deriving classification indices to ensure temporal stability (Step 1.a in Section 3.4.1). The following results document the differences between the refined maps of forest probabilities (CPN outputs), and thus illustrate the level of interoperability between the two sensors within NI-LCCP. Originally, the probability of a Landsat TM/ETM+ pixel being correctly classified (error rate term Q_2 in Eq. (3)) was set to 95.0 %. To

reflect the system's reduced accuracy when attempting to reproduce the base image using SAR data (see Table 4), this probability was here decreased to 90.0 % in the spatio-temporal model for epochs containing the PALSAR classifications.

As stated in Section 1.1, this work does not consider the use of SAR data with a view to improve on the existing Landsat-based products. Instead, the aim here is to address questions such as whether one dataset can be used to reproduce the results obtained with the other. To this purpose, two different scenarios of time series processing were considered, to provide various insights into the interoperability and potential influence of different sensors on the forest estimates.

4.4.1. Multi-temporal Scenario 1: independent processing

The first multi-temporal scenario corresponds to the case where both the optical and SAR datasets are processed independently. In other words, the four years of PALSAR data are processed by the spatio-temporal model, and these (SAR-only) results are then compared to the Landsat-only outputs obtained from the same four years of optical data. Table 5 contains the summary statistics for this scenario, which include the forest and non-forest amounts for each year over Tasmania, as well as the transitions between classes corresponding to cases of afforestation, deforestation and 'no change'.

Table 5. Summary statistics for outputs of the multi-temporal processing over Tasmania using the four year PALSAR time series (left) and four year Landsat time series (right). All values are given in km^2. The columns show the amounts of forest (F), non-forest (NF), and transitions between classes compared to the previous year, with 'F→NF' and 'NF→F' corresponding to deforestation and afforestation, respectively, and 'NC' indicating 'no change'.

year	PALSAR (4 years)					Landsat (4 years)				
	F	NF	F→NF	NF→F	NC	F	NF	F→NF	NF→F	NC
2007	48,967.3	19,563.6	-	-	-	46,351.8	22,179.1	-	-	-
2008	48,884.3	19,646.6	262.1	179.1	68,089.6	45,829.5	22,701.4	825.8	303.5	67,401.6
2009	48,878.7	19,652.2	208.5	202.9	68,119.5	45,620.6	22,910.3	469.6	260.7	67,800.6
2010	48,971.0	19,559.9	141.0	233.2	68,156.7	45,467.8	23,063.1	432.8	280.0	67,818.1

Table 5 indicates that the PALSAR time series consistently leads to increased forest totals compared to the Landsat results, with an additional amount of about 3,100 km^2 on average (corresponding to about 4.5 % of the total processed land area). A paired two-sample *t*-test indicates that this difference in forest amounts is statistically significant ($p = 0.0005$). Compared to the single-date results in Table 3, the model has thus resolved the (spatial and temporal) uncertainties in a way that confirms the consistent bias of PALSAR towards forest. Also, and more importantly from a carbon accounting perspective, differences in the deforestation and afforestation amounts can be quite large between the two time series. The areas of deforestation (F→NF) detected with the Landsat data are up to three times larger than those shown in the PALSAR results. While the areas of afforestation (NF→F) are in better agreement, the Landsat figure for 2008 is still nearly twice that of PALSAR. While some genuine differences might result from different acquisition dates between the SAR and optical datasets, such discrepancies when assessing these class transitions are quite substantial and would thus necessitate careful consideration in the frame of an operational multi-sensor forest monitoring system. A visual inspection of the change layers showed that these discrepancies are mainly due to the following reasons.

- Limited ability to detect certain types of deforestation events with PALSAR data, such as harvested plantations and light to moderate fire events, thus also reducing the ability to detect subsequent reforestation events.
- Timing of afforestation: PALSAR identifies regenerating regions (e.g., growing plantations) as reforestation 1 to 2 years earlier than Landsat, thus contributing to the afforestation counts of different epochs.
- Inaccuracies in any of the single-date Landsat or PALSAR classifications, leading to erroneous afforestation or deforestation in the corresponding multi-temporal outputs.
- Missing data in various years of the Landsat time series (due to clouds, sensor deficiencies, etc.), which precludes a proper inference of the timing of forest change in affected areas, especially for short time series such as the one considered in this scenario.

4.4.2. Multi-temporal Scenario 2: switch between sensors

The second scenario of multi-temporal processing compares the spatio-temporal model outputs from the following two time series:

1) 19 epochs of Landsat data from 1972 to 2010,
2) 15 epochs of Landsat data (1972 – 2006) followed by 4 years of PALSAR data (2007 – 2010).

This scenario provides insights into the impacts of different sensor biases, and thus into the interoperability of PALSAR and Landsat when used interchangeably within a single time series. Results similar to Table 5 are here presented graphically in Figure 4, illustrating how the estimates fluctuate during, before and after the transition (2007). Full

interoperability between sensors would be expected to lead to very similar curves of forest, non-forest and change extents for the Landsat-only (dashed lines) and mixed Landsat – PALSAR (solid lines) time series.

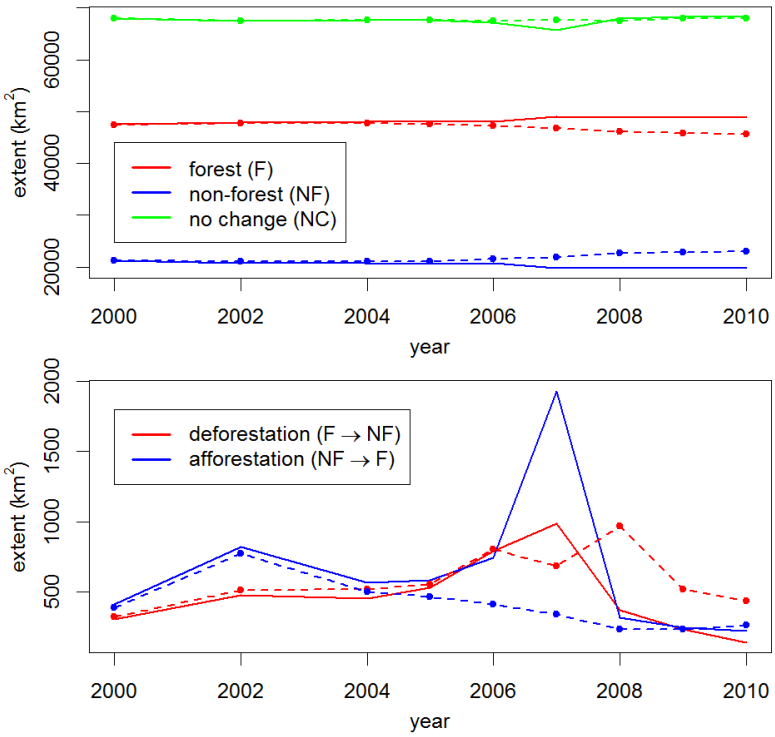

Figure 4. Summary statistics for the 19 year multi-temporal processing, comparing the mixed Landsat – PALSAR time series outputs (solid lines) to those of the Landsat-only time series (dashed lines). The two time series yield results that are virtually identical for the years prior to 2000 (ten epochs between 1972 and 1998), and are thus not shown here. Forest (F) and non-forest (NF) counts represent yearly quantities, while 'no change' (NC), deforestation and afforestation amounts correspond to changes from one epoch to the next.

Figure 4 again identifies some large differences between the two times series. For the mixed PALSAR – Landsat results (solid lines), significant spikes in the deforestation and afforestation amounts can be observed in 2007, due to the discrepancies between the SAR and optical F/NF classifications. At that point, the model essentially "adjusts" these regions of disagreement, leading to the corresponding areas being treated as forest conversion. For instance, urban regions incorrectly labelled as forest in the PALSAR classifications contribute to the inflated afforestation counts in the SAR – optical model outputs for 2007 (transition from the correctly labelled Landsat time series). Some of this adjustment process can also be seen to occur in the years before and after 2007, with deforestation/afforestation discrepancies between the two time series being larger than in other epochs. By 2010, the deforestation and afforestation amounts of the mixed time series (138.0 and 223.9 km^2, respectively) have "settled" to similar SAR-based values as shown in Table 5 for the PALSAR-only time series; a similar observation applies to the forest and non-forest amounts (48,996.3 and 19,733.5 km^2, respectively).

4.5. Comparative assessment of change products

With an emphasis on carbon tracking, we further quantify the significance of discrepancies between typical change products derived from the Landsat and PALSAR-based multi-temporal outputs at various spatial scales, using the three metrics defined in Section 3.5. In the case of Scenario 1, change maps are calculated by comparison of the 2007 and 2010 CPN class labels (corresponding to the beginning and end of the time series) for both the Landsat-only and PALSAR-only time series. With Scenario 2, the 2005 and 2009 epochs were selected to generate change information; the rationale here is that a change map calculated using epochs 2 years before and after the switch from Landsat to PALSAR in the mixed time series would provide most insight into the impact of the sensor change, as compared to the Landsat-only time series.

For these analyses, a grid of fifty-five 10 km × 10 km areal samples (100 km^2, or 160,000 pixels each) was established across Tasmania, and the amounts of deforestation, afforestation and 'no change' were subsequently recorded for each sample. In the following results, the optical change map is considered to be the reference data in both scenarios, with the PALSAR-only (Scenario 1) and mixed SAR – optical (Scenario 2) change maps treated as those being evaluated. This designation is arbitrary and does not impact conclusions about classification similarities for change maps.

Table 6 presents the results from the first metric, which evaluates the similarities of Tasmania-wide change maps by comparing the optical estimates (census) with the SAR-based confidence limits for each landcover change type. These results suggest that there are significant differences between the change extents estimated on the basis of optical and PALSAR data. For Scenario 1, estimates for the deforestation and 'no change' classes are significantly different (the corresponding Landsat estimates are not contained within the SAR-based 95 % confidence interval), although there appears to be no difference between the afforestation estimates (p = 0.374). With Scenario 2, the afforestation and 'no change' cases are both significantly different, while there is a non-significant difference between the optical and SAR-based deforestation amounts (p = 0.116). As already observed in Section 4.4.2, the increased SAR-based afforestation extents for Scenario 2 can here also be explained by the discrepancies between the optical and PALSAR single-date classifications, and the resulting "adjustment" made by the spatio-temporal model in these areas in 2007. Observations similar to those listed in Section 4.4.1 here also explain the lower deforestation amounts obtained with the PALSAR time series in Scenario 1.

Table 6. Confidence intervals for Tasmania-wide estimates of landcover change, based on a set of 55 areal samples. All values (except *p*-values) are given in km^2. 'Landsat estimates' are obtained from the Landsat-only time series (in both scenarios), whereas 'SAR-based estimates' are from the PALSAR-only (Scenario 1) and the mixed SAR – optical (Scenario 2) time series. In the last column, *p*-values indicate the statistical significance of both (mean) estimates being identical (e.g., p = 0.001 indicates a statistically significant difference with 99.9 % confidence).

scenario	change type	Landsat estimate (Tas.-wide census)	SAR-based estimate (**mean**) with 95 % confidence interval	*p*-value on mean difference
Scenario 1 (2007 – 2010 change map)	deforestation	1,634.9	299.7 – **686.2** – 1,072.7	0.000
	afforestation	751.0	399.0 – **642.3** – 885.6	0.374
	no change	66,145.0	66,675.8 – **67,114.2** – 67,552.5	0.000
Scenario 2 (2005 – 2009 change map)	deforestation	2,779.4	1,341.9 – **2,141.6** – 2,941.4	0.116
	afforestation	1,010.2	2,839.1 – **3,921.2** – 5,003.2	0.000
	no change	64,940.3	61,467.4 – **62,625.5** – 63,783.6	0.000

Results from the second metric in Table 7 provide a regional (100 km^2) rather than global assessment of similarities between optical and SAR-based change maps. Here, *p*-values represent the probability (statistical significance) of rejecting the null hypothesis that *kappa* ≠ 0. For instance, p = 0.01 would indicate a 99.0 % confidence that the agreement between the two change maps is statistically different from random. For both scenarios, the significance of global *kappa* (p = 0.00) in Table 7 indicates that the agreement between the optical and SAR change maps is statistically relevant, as do the global accuracies and the significance of the conditional *kappa* values (which evaluate similarities between individual change types). However, the user's and producer's accuracies demonstrate that this is mainly due to the overwhelming agreement of the 'no change' class, which covers over 96 % of Tasmania according to the optical estimates (Table 6). In Scenario 1, the difference between the user's and producer's accuracy for deforestation suggests that a large amount of deforestation will be identified in some regions using optical data, but PALSAR change maps will only agree with roughly one third of this. Results for afforestation with Scenario 2 suggest the opposite: within each region, relatively little afforestation will be identified using optical data, but SAR-based change maps will agree with most of the afforestation identified. This latter observation is consistent with results in Table 6, which indicate that about four times more afforestation is identified on the SAR-based change map than on the optical map. With Scenario 2, the relatively high user's accuracy for afforestation indicates a high level of spatial coincidence of that change class at a regional level.

Table 7. Results from analyses based on areal confusion matrices (computed from 55 areal samples) comparing the Landsat-only change maps to the PALSAR-only (Scenario 1) and mixed PALSAR – Landsat (Scenario 2) change maps.

scenario	global *kappa* (*p*-value)	global accuracy	accuracy type	deforestation	afforestation	no change
Scenario 1 (2007 – 2010 change map)	0.53 (0.00)	97.6 %	user's	33.4 %	54.3 %	99.6 %
			producer's	78.5 %	52.2 %	98.2 %
			conditional kappa (*p*)	0.33 (0.00)	0.54 (0.00)	0.78 (0.00)
Scenario 2 (2005 – 2009 change map)	0.58 (0.00)	94.2 %	user's	56.6 %	90.3 %	95.9 %
			producer's	74.2 %	28.4 %	99.0 %
			conditional kappa (*p*)	0.55 (0.00)	0.90 (0.00)	0.54 (0.00)

Results from the third metric in Table 8 evaluate the accuracy of exact locations (individual pixels) using the conventional pixel-based confusion matrix. Here, the sample size is 8.8 million (55 areal samples of 160,000 pixels each), a not unreasonable sample size given the need to adequately sample the relatively rare deforestation and afforestation classes. Again, global and conditional *kappa* values demonstrate a statistically relevant relationship ($p = 0.00$) between the optical and SAR-based landcover change maps. The global accuracy is also above 90 %, although this result is here also related to the prevalence of the 'no change' class. Despite these results, the user's and producer's accuracies are relatively low, suggesting a poor agreement (though statistically significant) of individual pixels.

Table 8. Results from analyses based on pixel-based confusion matrices (using 8.8 million pixels) comparing the Landsat-only change maps to the PALSAR-only (Scenario 1) and mixed PALSAR – Landsat (Scenario 2) change maps.

scenario	global *kappa* (*p*-value)	global accuracy	accuracy type	deforestation	afforestation	no change
Scenario 1 (2007 – 2010 change map)	0.11 (0.00)	95.4 %	user's	9.3 %	9.2 %	98.3 %
			producer's	22.0 %	8.8 %	97.0 %
			conditional kappa (*p*)	0.08 (0.00)	0.08 (0.00)	0.15 (0.00)
Scenario 2 (2005 – 2009 change map)	0.28 (0.00)	90.0 %	user's	28.8 %	64.6 %	93.1 %
			producer's	37.7 %	20.4 %	96.1 %
			conditional kappa (*p*)	0.27 (0.00)	0.63 (0.00)	0.22 (0.00)

Statistically, some of the above results appear to be somewhat at odds. Global confidence intervals (Table 6) indicate a significant disagreement for Tasmania-wide landcover change, while global and conditional *kappa* values (Table 7 and Table 8) point to a statistically significant relationship between the change maps produced from optical and SAR-based data at the regional and local scale. Interestingly, this suggests that at these smaller scales there could be some reasonable level of interoperability between the optical and SAR data for all change classes. Over larger areas, however, the optical and SAR-based change estimates will be significantly biased, and taken altogether, these results in fact indicate that the SAR-based time series produce change maps with significantly less (Scenario 1) or more (Scenario 2) change globally compared to the optical maps.

5. Concluding discussion

With the continuous expansion of remote sensing datasets available for large-scale forest mapping and monitoring (e.g., Landsat 8, Sentinel and ALOS-2 missions), investigating the ability to draw on information provided by multiple sensors will continue to attract much research interest. This is further motivated by potential issues of data continuity due to sensor failure or modification, and by difficulties in establishing a consistent optical archive in regions strongly affected by cloud cover, such as tropical countries.

The present work was concerned with the integration of SAR data within Australia's established Landsat-based NI-LCCP framework. It highlighted some of the main operational issues that will need to be closely considered in the development of such large-scale SAR – optical systems for forest monitoring, such as co-registration issues, interoperability and complementarity of the datasets, need for stratified processing, and quantifying the relevance of different SAR data and related texture information. This work thus provides pertinent insights for countries looking at making use of large-scale medium-resolution SAR products (current and future), such as JAXA's worldwide PALSAR mosaics (Shimada and Ohtaki, 2010), as part of existing optical-based forest monitoring frameworks. While the current work focused on the state of Tasmania, the stratified approach implemented within NI-LCCP allows for a straightforward extension of these results to larger geographical extents.

The use of a consistent methodology to process both the Landsat and SAR time series allowed us to gain important insights into their respective forest mapping characteristics within NI-LCCP. As can be expected, complications will inevitably arise when substituting data from a different sensor into an existing (legacy) framework, with outcomes influenced by the specific biases introduced by each type of data (Furby and Wu, 2009). While a good agreement in overall forest extents was obtained with the optical and SAR datasets, significant and non-negligible differences were also identified when considering the specific case of forest conversion at a global scale, thereby compromising a fully interoperable use of SAR and optical data for forest carbon tracking purposes within the considered framework. A possible approach that could circumvent part of this issue would be to fuse the SAR and optical information at the data level, by using the combined datasets as input to a joint classification scheme (see, e.g., Lehmann et al., 2011). This would essentially place more emphasis on the complementary nature of the datasets, rather than their interoperability. Results presented in Section 4.1 indeed demonstrate a significant complementarity of the optical and SAR datasets. This would however also require the datasets to be as temporally coincident as possible in each epoch, a condition likely to impose important operational constraints and additional costs in the development of a multi-sensor framework.

The methods and results in this work were presented in the frame of an existing scheme that naturally lends itself to the integration of new datasets. Ideally, a joint SAR – optical monitoring system built from scratch would use a base image (reference data for the single-date classifications) derived on the basis of both the SAR and optical data. This however implies that the Landsat-based classifications would have to be re-generated for all epochs since 1972, as opposed to using the existing NI-LCCP maps as was done in this paper. The sheer amount of work involved with this approach renders this task well beyond the scope of this work.

Further potential improvements to the approach used here could be achieved in various ways. The use of different classification algorithms might improve the single-date SAR classifications to some extent (Mitchell et al., 2011a; O'Connell and Caccetta, 2009). Further SAR-specific information, such as the SAR entropy or coherence, for instance, could also allow further refinements of the forest classifications. The use of dense time series of C-band observations has also been shown to provide relevant forest monitoring information (Hoekman, 2012), and further research could investigate the integration of such (intra-annual) data within the proposed framework. The use of further ancillary data for classification (e.g., elevation, terrain slope and orientation, forestry polygons, masks of water and urban areas, etc.) would also likely contribute to an improvement of the forest maps (Mitchell et al., 2014, 2011a). This could however also represent an impediment to the extension of this framework to larger geographical areas, where this type of information might not be readily available.

Thus, while an increased level of SAR – optical interoperability might be achievable within the considered framework through such methodological changes, this would likely come at the cost of additional resources and processing needs in an operational setting (in contrast to the "low cost" approach investigated in this work, see Section 1.1). Also, some of the main conclusions reached here in terms of data interoperability for operational forest monitoring are likely to remain (see, e.g., Figure 3). SAR and optical sensors intrinsically observe the Earth's surface in different ways, with SAR responding to forest structure and dielectric content, and optical sensors relying on a more biochemical response. Some discrepancies in the PALSAR and Landsat forest classifications are therefore inevitable and inherent to the way in which radar and optical sensors measure the ground cover.

Acknowledgement

This Tasmanian National Demonstrator Project was conducted as part of the GEO Forest Carbon Tracking task. The PALSAR data were provided by JAXA and Geoscience Australia, and the RADARSAT-2 data were provided by the Canadian Space Agency, both within the framework of GEO-FCT. The authors gratefully acknowledge the Australian Department of Climate Change and Energy Efficiency for funding and data provision. Forestry Tasmania also provided valuable field assistance, logistical support and strategic advice as part of this work. Dr. Xiaoliang Wu (CSIRO Digital Productivity Flagship) is also acknowledged for his help with the PALSAR data processing. We would also like to thank three anonymous reviewers of this paper for their positive feedback and constructive comments.

References

ADE, 2014. National Inventory Report 2012, Volume 2. Australian Department of the Environment (ADE), Commonwealth of Australia, Canberra, Australia.

Brack, C., Richards, G., Waterworth, R., 2006. Integrated and comprehensive estimation of greenhouse gas emissions from land systems. Sustainability Science 1, 91–106.

Caccetta, P., 1997. Remote sensing, geographic information systems (GIS) and Bayesian knowledge-based methods for monitoring land condition (Ph.D. thesis). Curtin University of Technology, School of Computing, Perth, Australia.

Caccetta, P., Furby, S., O'Connell, J., Wallace, J., Wu, X., 2007. Continental monitoring: 34 years of land cover change using Landsat imagery, in: International Symposium on Remote Sensing of Environment. San José, Costa Rica, pp. 1–4.

Caccetta, P., Waterworth, R., Furby, S., Richards, G., 2010. Monitoring Australian continental land cover changes using Landsat imagery as a component of assessing the role of vegetation dynamics on terrestrial carbon cycling, in: European Space Agency Living Planet Symposium. Bergen, Norway, pp. 1–7.

Campbell, N., 1994. Canonical variate analysis – A general model formulation. Australian and New Zealand Journal of Statistics 26, 86–96.

Campbell, N., Wu, X., 2008. Gradient cross correlation for sub-pixel matching, in: Congress of the International Society for Photogrammetry and Remote Sensing. Beijing, China, pp. 1065–1070.

Canty, M.J., 2014. Image Analysis, Classification and Change Detection in Remote Sensing. CRC Press.

Cohen, J., 1960. A Coefficient of Agreement for Nominal Scales. Educational and Psychological Measurement 20, 37–46.

Congalton, R.G., Green, K., 2009. Assessing the Accuracy of Remotely Sensed Data: Principles and Practices, 2nd ed. CRC Press, Taylor & Francis Group, Boca Raton, FL.

DeFries, R., Achard, F., Brown, S., Herold, M., Murdiyarso, D., Schlamadinger, B., de Souza Jr., C., 2007. Earth observations for estimating greenhouse gas emissions from deforestation in developing countries. Environmental Science & Policy 10, 385–394.

De Oliveira Pereira, L., da Costa Freitas, C., Sant'Anna, S.J.S., Lu, D., Moran, E.F., 2013. Optical and radar data integration for land use and land cover mapping in the Brazilian Amazon. GIScience & Remote Sensing 50, 301–321.

Dong, J., Xiao, X., Chen, B., Torbick, N., Jin, C., Zhang, G., Biradar, C., 2013. Mapping deciduous rubber plantations through integration of PALSAR and multi-temporal Landsat imagery. Remote Sensing of Environment 134, 392–402.

DPIPWE, 2009. Tasmanian Vegetation Monitoring and Mapping Program: TASVEG 2.0 Metadata (release date: 19th February 2009). Department of Primary Industries, Parks, Water, and Environment (DPIPWE), Vegetation Conservation Section, Tasmania.

EEA, 2007. CLC2006 technical guidelines (Technical report No 17). European Environment Agency (EEA), Copenhagen, Denmark.

Furby, S., 2002. Land cover change: specification for remote sensing analysis. National Carbon Accounting System, Technical Report no. 9, Australian Greenhouse Office, Canberra.

Furby, S., Caccetta, P., Wu, X., Chia, J., 2008. Continental scale land cover change monitoring in Australia using Landsat imagery, in: International Earth Conference: Studying, Modeling and Sense Making of Planet Earth. Mytilene, Lesvos, Greece, pp. 1–8.

Furby, S., Campbell, N., 2001. Calibrating images from different dates to "like-value" digital counts. Remote Sensing of Environment 77, 186–196.

Furby, S., Wu, X., 2009. Evaluation of alternative sensors for a Landsat-based monitoring program, in: Jones, S., Reinke, K. (Eds.), Innovations in Remote Sensing and Photogrammetry, Lecture Notes in Geoinformation and Cartography. Springer-Verlag, Berlin Heidleberg, pp. 75–90.

Haralick, R.M., Shanmugam, K., Dinstein, I., 1973. Textural Features for Image Classification. IEEE Transactions on Systems, Man and Cybernetics SMC-3, 610–621.

Harris, S., Kitchener, A., 2005. From Forest to Fjaeldmark: Descriptions of Tasmania's Vegetation. Department of Primary Industries, Water and Environment, Printing Authority of Tasmania, Hobart.

Herold, M., Johns, T., 2007. Linking requirements with capabilities for deforestation monitoring in the context of the UNFCCC-REDD process. Environmental Research Letters 2, 1–7.

Hoekman, D., 2012. Key science questions: Optimising information extraction from C-band SAR, in: GEO FCT Science and Data Summit #3. Arusha, Tanzania.

Homer, C., Huang, C., Yang, L., Wylie, B., Coan, M., 2004. Development of a 2001 National Land-Cover Database for the United States. Photogrammetric Engineering & Remote Sensing 70, 829–840.

JAXA, 2014. New global 50m-resolution PALSAR mosaic and forest/non-forest map [WWW Document]. URL http://www.eorc.jaxa.jp/ALOS/en/palsar_fnf/fnf_index.htm (accessed May 26, 2014).

Kiiveri, H., Caccetta, P., Campbell, N., Evans, F., Furby, S., Wallace, J., 2003. Environmental monitoring using a time series of satellite images and other spatial data sets, in: Denison, D., Hansen, M., Holmes, C., Mallick, B., Yu, B. (Eds.), Nonlinear Estimation and Classification, Lecture Notes in Statistics. Springer-Verlag, New York, pp. 49–62.

Kuplich, T.M., Curran, P.J., Atkinson, P.M., 2005. Relating SAR image texture to the biomass of regenerating tropical forests. International Journal of Remote Sensing 26, 4829–4854.

LAPAN, 2014. The Remote Sensing Monitoring Program of Indonesia's National Carbon Accounting System: Methodology and Products, Version 1. LAPAN-IAFCP, Jakarta.

Lehmann, E.A., Caccetta, P.A., Zhou, Z.-S., McNeill, S.J., Wu, X., Mitchell, A.L., 2012a. Joint Processing of Landsat and ALOS-PALSAR Data for Forest Mapping and Monitoring. IEEE Transactions on Geoscience and Remote Sensing 50, 55–67.

Lehmann, E.A., Zhou, Z., Caccetta, P., Milne, A., Mitchell, A., Lowell, K., Held, A., 2012b. Forest mapping and monitoring in Tasmania using multi-temporal Landsat and ALOS-PALSAR data, in: IEEE International Geoscience and Remote Sensing Symposium. pp. 6431–6434.

Lehmann, E., Caccetta, P., Zhou, Z.S., Mitchell, A., Tapley, I., Milne, A., Held, A., Lowell, K., McNeill, S., 2011. Forest discrimination analysis of combined Landsat and ALOS-PALSAR data, in: International Symposium for Remote Sensing of the Environment. Sydney, Australia, pp. 1–5.

Lisini, G., Gamba, P., Dell'Acqua, F., Holecz, F., 2011. First results on road network extraction and fusion on optical and SAR images using a multi-scale adaptive approach. International Journal of Image and Data Fusion 2, 363–375.

Longépé, N., Rakwatin, P., Isoguchi, O., Shimada, M., Uryu, Y., Yulianto, K., 2011. Assessment of ALOS PALSAR 50 m Orthorectified FBD Data for Regional Land Cover Classification by Support Vector Machines. IEEE Transactions on Geoscience and Remote Sensing 49, 2135–2150.

Lu, D., Li, G., Moran, E., 2014. Current situation and needs of change detection techniques. International Journal of Image and Data Fusion 5, 13–38.

MacKay, R., Campbell, N., 1982. Variable selection techniques in discriminant analysis – Description. British Journal of Mathematical and Statistical Psychology 35, 1–29.

Mitchell, A.L., Milne, A., Tapley, I., Lowell, K., Caccetta, P., Lehmann, E., Zhou, Z.-S., Held, A., 2011a. Interoperability of radar and optical data for forest information assessment, in: IEEE International Geoscience and Remote Sensing Symposium. Vancouver, BC, Canada, pp. 1397–1400.

Mitchell, A.L., Milne, A., Tapley, I., Lowell, K., Caccetta, P., Lehmann, E., Zhou, Z.-S., Held, A., 2011b. Key outcomes of the Tasmania "National Demonstrator": A project for the GEO Forest Carbon tracking task, in: International Symposium on Remote Sensing of Environment. Sydney, Australia.

Mitchell, A.L., Tapley, I., Milne, A., Williams, M., Zhou, Z.-S., Lehmann, E., Caccetta, P., Lowell, K., Held, A., 2014. C- and L-band SAR interoperability: Filling the gaps in continuous forest cover mapping in Tasmania. Remote Sensing of Environment (accepted for publication).

Morel, A.C., Fisher, J.B., Malhi, Y., 2012. Evaluating the potential to monitor aboveground biomass in forest and oil palm in Sabah, Malaysia, for 2000–2008 with Landsat ETM+ and ALOS-PALSAR. International Journal of Remote Sensing 33, 3614–3639.

O'Connell, J., Caccetta, P., 2009. Testing of alternate classification procedures within an operational, satellite based, forest monitoring system, in: Jones, S., Reinke, K. (Eds.), Innovations in Remote Sensing and Photogrammetry, Lecture Notes in Geoinformation and Cartography. Springer-Verlag, Berlin Heidleberg, pp. 121–132.

Otukei, J.R., Blaschke, T., Collins, M., Maghsoudi, Y., 2011. Analysis of ALOS PALSAR and TerraSAR-X data for protected area mapping: A case of the Bwindi Impenetrable National Park-Uganda, in: IEEE International Geoscience and Remote Sensing Symposium. pp. 348–351.

Peters, D., Thackway, R., 1998. A New Biogeographic Regionalisation for Tasmania. Commonwealth of Australia, Parks & Wildlife Service, Tasmania.

Pontius, R.G., Cheuk, M.L., 2006. A generalized cross-tabulation matrix to compare soft-classified maps at multiple resolutions. International Journal of Geographical Information Science 20, 1–30.

Roswintiarti, O., Kustiyo, Tjahyaningsih, A., Furby, S., Wallace, J., 2013. Indonesia's National Carbon Accounting remote sensing program - A national system for monitoring forest changes, in: IEEE International Geoscience and Remote Sensing Symposium. pp. 3930–3933.

Shimada, M., Isoguchi, O., Motooka, T., Shiraishi, T., Mukaida, A., Okumura, H., Otaki, T., Itoh, T., 2011. Generation of 10m resolution PALSAR and JERS-SAR mosaic and forest/non-forest maps for forest carbon tracking, in: IEEE International Geoscience and Remote Sensing Symposium. Vancouver, BC, Canada, pp. 3510–3513.

Shimada, M., Itoh, T., Motooka, T., Watanabe, M., Shiraishi, T., Thapa, R., Lucas, R., 2014. New global forest/non-forest maps from ALOS PALSAR data (2007–2010). Remote Sensing of Environment 19 pages. doi:10.1016/j.rse.2014.04.014

Shimada, M., Ohtaki, T., 2010. Generating Large-Scale High-Quality SAR Mosaic Datasets: Application to PALSAR Data for Global Monitoring. IEEE Journal of Selected Topics in Applied Earth Observations and Remote Sensing 3, 637–656.

Sutton, M.A., Orteu, J.J., Schreier, H., 2009. Image Correlation for Shape, Motion and Deformation Measurements: Basic Concepts, Theory and Applications. Springer, New York, USA.

Vaglio Laurin, G., Liesenberg, V., Chen, Q., Guerriero, L., Del Frate, F., Bartolini, A., Coomes, D., Wilebore, B., Lindsell, J., Valentini, R., 2013. Optical and SAR sensor synergies for forest and land cover mapping in a tropical site in West Africa. International Journal of Applied Earth Observation and Geoinformation 21, 7–16.

Wolter, P.T., Townsend, P.A., 2011. Multi-sensor data fusion for estimating forest species composition and abundance in northern Minnesota. Remote Sensing of Environment 115, 671–691.

Zhang, J., Tan, T., 2002. Brief review of invariant texture analysis methods. Pattern Recognition 35, 735–747.

Zhang, Y., 2001. Texture-Integrated Classification of Urban Treed Areas in High-Resolution Color-Infrared Imagery. Photogrammetric Engineering and Remote Sensing 67, 1359–1365.

Zhou, Z.S., Lehmann, E., Wu, X., Caccetta, P., McNeill, S., Mitchell, A., Milne, A., Tapley, I., Lowell, K., 2011. Terrain slope correction and precise registration of SAR data for forest mapping and monitoring, in: International Symposium for Remote Sensing of the Environment. Sydney, Australia, pp. 1–4.